Dear Author,

Please, note that changes made to the HTML content will be added to the article before publication, but are not reflected in this PDF.

Note also that this file should not be used for submitting corrections.

Nano Energy ∎ (∎∎∎∎) ∎∎∎–∎∎∎

Contents lists available at ScienceDirect

Nano Energy

journal homepage: www.elsevier.com/locate/nanoen

Ethanol reduced molybdenum trioxide for Li-ion capacitors

Tianqi Li [a], Majid Beidaghi [b], Xu Xiao [a], Liang Huang [a], Zhimi Hu [a], Wanmei Sun [a], Xun Chen [a], Yury Gogotsi [c,*], Jun Zhou [a]

[a] Wuhan National Laboratory for Optoelectronics, Huazhong University of Science and Technology, Wuhan 430074, China
[b] Department of Materials Engineering, Auburn University, 275 Wilmore Labs, Auburn, Al 36849, USA
[c] Department of Materials Science and Engineering and A. J. Drexel Nanomaterials Institute, Drexel University, 3141 Chestnut Street, Philadelphia, PA 19104, USA

ARTICLE INFO

Article history:
Received 29 February 2016
Received in revised form
4 May 2016
Accepted 5 May 2016

Keywords:
Molybdenum trioxide
Supercapacitor
Li-Ion capacitor
Energy storage

ABSTRACT

Orthorhombic molybdenum trioxide (α-MoO_3) is a layered oxide with promising performance as electrode material for Li-ion capacitors. In this study, we show that expansion of the interlayer spacing (by ~0.32 Å) of the structure along the b-axis, introduced by partial reduction of α-MoO_3 and formation of MoO_{3-x} (x=0.06–0.43), results in enhanced diffusion of Li ions. Freestanding hybrid electrodes made of MoO_{3-x} nanobelts and carbon nanotubes show excellent electrical conductivity. The combination of increased interlayer spacing and enhanced electron transport leads to high gravimetric and volumetric capacitances of about 420 F/g or F/cm^3 and excellent cycle life of binder-free MoO_{3-x} electrodes.

1. Introduction

Electrochemical capacitors (ECs) [1–6] are energy storage devices with higher power densities comparing to batteries. Electric double-layer capacitors (EDLCs) are the most common type of ECs [3], which store charge electrostatically at the electrode/electrolyte interface without any charge transfer. On the contrary, batteries [7–9] only benefit from the Faraday currents from redox reactions introducing phase transformations (nickel metal hydride battery [10,11] and lead-acid battery [12]) or intercalation reactions (Li-ion battery [13]). By studying the charge storage mechanism in ruthenium dioxide (RuO_2), Conway proposed the concept of redox current-induced pseudocapacitance [5]. Transition metal oxides such as RuO_2 and manganese dioxide (MnO_2) [14–16] show pseudocapacitive properties and are superior to EDLCs in terms of gravimetric and volumetric capacitance in aqueous electrolytes. However, the charge storage mechanism of pseudocapacitors limited to surface redox reaction determines the total amount of energy stored. Generally, volumetric capacitance is of significance for applications such as portable electronics and electric vehicles (EVs) due to the limited available space for the energy storage device. In order to achieve a higher volumetric capacitance, researchers are focusing on developing high mass density carbon or layered compounds such as 2D carbides (MXenes) [17] and MoS_2 [18] for EC electrodes [17,19]. It should be noted that these materials exhibit very high volumetric capacitances, but lower gravimetric capacitances compared to transition metal oxides. It is challenging to simultaneously obtain high gravimetric and volumetric capacitances.

Orthorhombic molybdenum trioxide (α-MoO_3) with a layered structure and redox active surface has been widely reported as a promising electrode material for ECs [20] and Li-ion batteries [21–23]. Previously, we reported amorphous MoO_{3-x}/WO_{3-x} hybrid structures, [24] which showed excellent gravimetric capacitance due to surface redox reactions. Later, we reported on hydrogenated MoO_3 with a high volumetric capacitance when used in an aqueous Li-ion capacitor [25] and in sea water electrolyte [26]. Unfortunately, the working potential window (V) for aqueous electrolytes is limited by electrolysis of water, which limits the energy (E) and power (P) of the supercapacitors ($E=CV^2/2$, $P=V^2/4R$, where C is capacitance and R is resistance). The working voltage window of ECs can be extended by using organic electrolytes. [27,28] Moreover, the electrode structure has an important effect of capacitive performance, which was not studied intensively previously. By using nanocrystalline electrodes, Dunn et al. demonstrated the intercalation process in ordered mesoporous MoO_3 resulting in charge storage of 605 C/g in a 2 V voltage window in an electrolyte of 1 M $LiClO_4$ in propylene carbonate [20].

Although α-MoO_3 has showed some promise, its low rate capability and poor cycling life [29,30] impose restrictions on its

* Corresponding author.
E-mail addresses: gogotsi@drexel.edu (Y. Gogotsi), jun.zhou@mail.hust.edu.cn (J. Zhou).

http://dx.doi.org/10.1016/j.nanoen.2016.05.004
2211-2855/

use. These issues can be ascribed to slow ion diffusion in the pores of the material and also poor electron transport due to low electronic conductivity of MoO_3. Both problems result in a low rate capability of the electrodes, while the latter problem also affects the cycling stability due to the nonuniform polarization of the electrodes.

Herein, we focus on enhancing the ionic and electronic conductivities of α-MoO_3 nanobelts by partial reduction of α-MoO_3 and introduction of oxygen vacancies into its structure. We found that the reduced form of α-MoO_3 (MoO_{3-x}) has a larger interlayer spacing along b-axis, which results in enhanced ion diffusion in the structure. Moreover, the MoO_{3-x} showed a higher electronic conductivity compared to α-MoO_3 before reduction. Freestanding and binder-free hybrid electrodes [31] of carbon nanotubes (CNTs) and MoO_{3-x} nanobelts show an excellent specific capacitance of 418 F/g including CNTs in $LiClO_4$ ethylene carbonate/dimethyl carbonate electrolyte (volumetric capacitance of 418 F/cm^3). Addition of CNTs to the electrode proved to be critical and about 90.2% of capacitance was retained after testing the hybrid electrode for 5000 cycles. Electrodes without CNT addition only retained 30% of their initial capacitance after the same number of cycles.

2. Experimental section

2.1. Materials

Mo powder (99.5%) and polyvinylidene fluoride (PVDF) were bought from Aladdin. The carbon black was bought from Alfa Aesar. Sodium dodecyl sulfate (SDS, 98%) and hydrogen peroxide (30%, H_2O_2) were purchased from Sinopharm Chemical Reagent Co., Ltd.

2.2. Synthesis

The α-MoO_3 nanobelts were synthesized via a hydrothermal process as reported elsewhere [25]. Briefly, 2 g molybdenum powder was added into 40 mL of deionized water and stirred to achieve a uniform mixture. Then, 20 mL of H_2O_2 was slowly dropped into the obtained mixed solution. After stirring for 30 min, the saffron yellow precursor solution was transferred to a Teflon lined stainless steel autoclave and heated at 180 °C for 12 h. The product precipitate was filtered and rinsed with deionized water, followed by drying at 60 °C for 12 h. For reduction of MoO_3 nanobelts, 0.3 g of MoO_3 was added into 15 mL of deionized water and 15 mL of ethanol in a Teflon lined stainless steel autoclave and

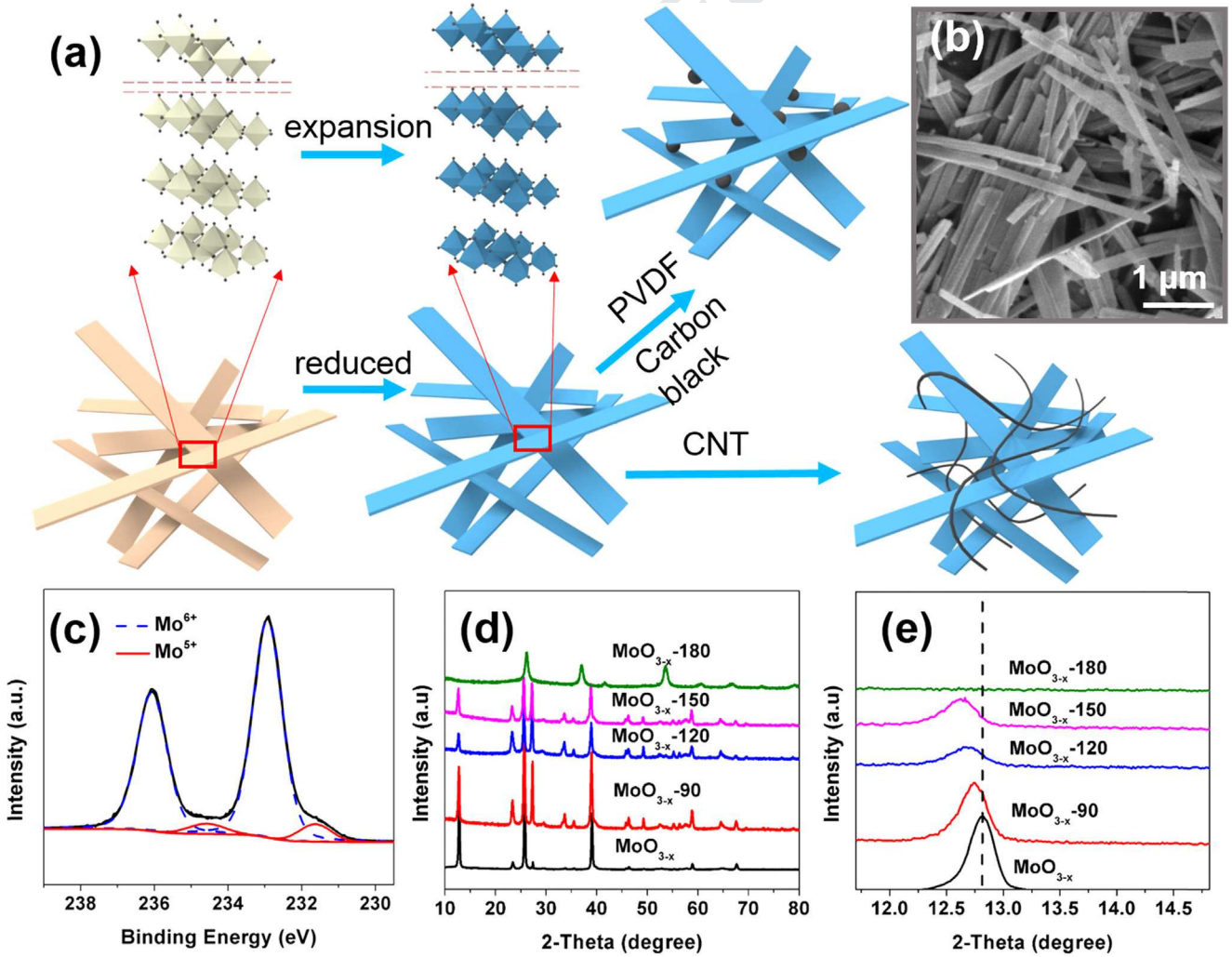

Fig. 1. (a) The schematic of MoO_3 reduction and electrode-preparation. (b) SEM image of MoO_3 reduced at 120 °C, (c) the Mo 3d XPS spectrum of MoO_{3-x}−120. (d) and (e) The XRD patterns of MoO_3 before and after reduction at different temperatures, (010) diffraction peaks of MoO_{3-x}−120 and MoO_{3-x}−150 nanobelts shifted to lower 2Θ values.

Please cite this article as: T. Li, et al., Ethanol reduced molybdenum trioxide for Li-ion capacitors, Nano Energy (2016), http://dx.doi.org/10.1016/j.nanoen.2016.05.004

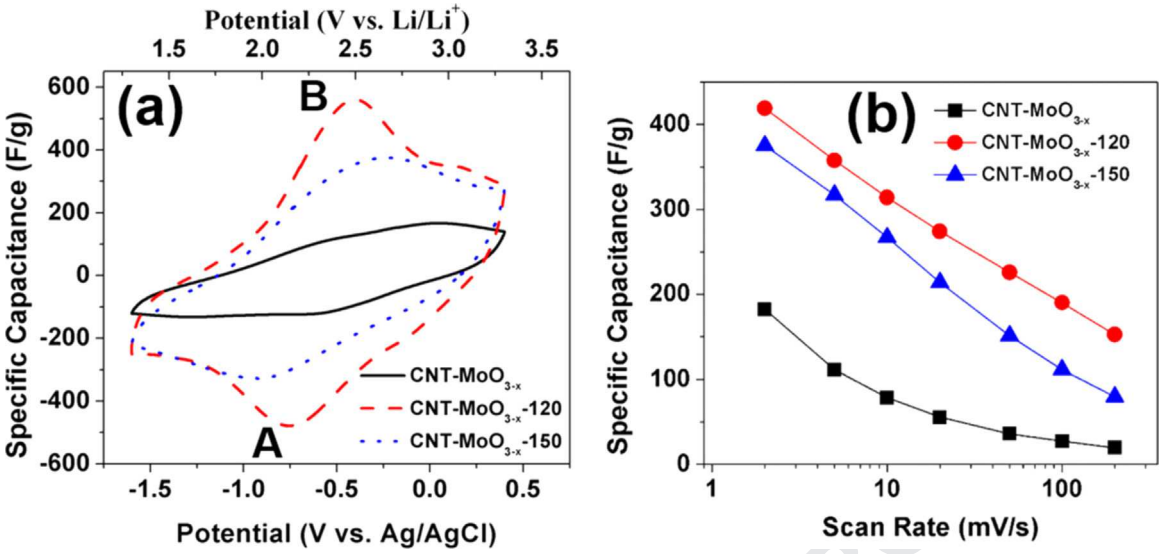

Fig. 2. (a) Cyclic voltammograms of CNT-MoO_{3-x}−120, CNT-MoO_{3-x}−150 and CNT-MoO_{3-x} at 20 mV/s. (b) The gravimetric capacitance vs. scan rate for CNT-MoO_{3-x}−120, CNT-MoO_{3-x}−150 and CNT-MoO_{3-x} from 2 mV/s to 200 mV/s.

heated at different temperatures. Sample notation includes the reduction temperature: for example, MoO_3 reduced at 120 °C is labeled as MoO_{3-x}−120.

2.3. Fabrication of electrodes

As shown in Fig. 1, the electrodes were prepared in two ways. For binder-free electrodes, MoO_{3-x} nanobelts, multiwalled carbon nanotubes (CNTs, prepared by a floating catalyst chemical vapor deposition; length ~500 μm) and sodium dodecyl sulfate (as surfactant) were added to deionized water in a 4:1:40 ratio. This mixture was the sonicated for 0.5 h and filtered on a Celgard membrane (3501 Coated PP, Celgard LLC, Charlotte, NC) using a standard vacuum filtration setup to form the binder-free free-standing electrodes. The conventional electrodes were fabricated by pasting a mixture of MoO_{3-x} nanobelts, PVDF, and carbon black at the 14:5:1 ratio on aluminum foil.

2.4. Characterization

The morphology and the structure of samples were studied by field-emission scanning electron microscopy (FE-SEM, FEI Nova 450 Nano) accompanied by energy-dispersive X-ray spectroscopy (EDS), high-resolution transmission electron microscopy (HR TEM, TECNAI G^2 20 U-TWIN), X-ray photoelectron spectroscopy (XPS, AXIS-ULTRA DLD-600W) and X-ray diffraction (XRD, X'Pert Pro, PANanalytical). N_2 adsorption–desorption isotherms were acquired on a Micromeretics ASAP 2000. Resistance measurements were conducted by the four-point probe method (ResTest v1, Jandel Engineering Ltd., Bedfordshire, UK). All the tested samples were freestanding films prepared the vacuum filtration of dispersed MoO_{3-x} nanobelts or their mixtures with CNTs. All electrochemical tests were carried out using a VMP-3 potentiostat (Biologic, France). For the typical three-electrode setup, an Ag/AgCl reference electrode, an oversized activated carbon (YP-50, Kuraray Chemical, Japan) counter electrode, and a Celgard separator (3501 Coated PP, Celgard LLC, Charlotte, NC) were used. All tests were conducted in a three-neck Swagelok cells (t-branch pipe, Swagelok, USA) were the working, the separator and the counter electrode were pressed between two stainless steal rods from two necks of the Swagelok cells and the third neck was used to place the reference electrode into the cell. The electrolyte was 1 M $LiClO_4$ in 1:1 mixture of ethylene carbonate and dimethyl carbonate. Electrochemical impedance measurements where performed in the frequency range from 10 mHz to 1 MHz with a potential amplitude of 5 mV at the open circuit potential. The capacitance (C) values were calculated by integrating the discharge portions of the cyclic voltammograms (CVs) and using the equation $C = \int(IV)/(m\nu\Delta V)$. The specific capacitance values were calculated considering the mass of all electrode components. The capacitance (C), charge storage (Q) and capacity (C_a) could be converted by the equations $C = QV$ ($V = 2$, *in this work*) and $C_a = Q/3.6$. The cycle life was tested by GCPL between the potential limits of −1.6 to 0.4 V versus Ag/AgCl, and the capacitance values were calculated from the slopes of the discharge curve.

3. Results and discussion

After hydrothermal treatment in ethanol, the color of MoO_3 powder was changed from light-gray to blue or black depending on the temperature of the hydrothermal treatment (Fig. 1a and Fig. S1a), suggesting a partial reduction of MoO_3 and introduction of oxygen vacancies in the structure [25]. Fig. 1b shows an SEM image of MoO_{3-x}−120 that has a similar morphology to the raw MoO_3 (Fig. S1b). The color of the MoO_{3-x} was darker after hydrothermal treatment at higher temperatures due to further reduction by ethanol. Although a complete understanding of the reduction of MoO_3 by this method needs further studies, we suggest the following reduction mechanism. The α-MoO_3 has a layered structure, which consists of bilayers of MoO_6 octahedra that are held together by van der Waals forces in the (010) direction. [32,33] During the hydrothermal treatment of the ethanol intercalated α-MoO_3 the Mo=O double bonds in between the layers in (010) direction can be reduced to Mo–O–H, resulting in an increased interlayer spacing and the observed color changes in the material. X-ray photoelectron spectroscopy (XPS) studies of the samples show two strong peaks corresponding to Mo^{6+} for sample before and after reduction, and also two new weaker peaks corresponding to Mo^{5+} that appears in the spectra for the reduced samples (Mo 3d spectrum in Fig. 1c and Fig. S2a). Also, comparison of the O1s spectra of the samples before and after reduction (Fig. S2) shows the appearance of a new peak after reduction, suggesting that Mo=O has changed to Mo–O–H [33]. By increasing the

reduction temperature, Mo–O–Mo bonds could be ruptured, leading to formation of cracks in nanobelts, such as the case of $MoO_{3-x}-150$ shown in Fig. S1c. For the samples treated at 180 °C ($MoO_{3-x}-180$), the Mo–O–Mo bonds were heavily ruptured resulting in the damage of nanobelts and forming nanopowder (Fig. S1d). X-ray diffraction (XRD) patterns of the untreated MoO_3 powder and samples treated at various temperatures are shown in Fig. 1d. The patterns of MoO_{3-x}, $MoO_{3-x}-90$, $MoO_{3-x}-120$, and $MoO_{3-x}-150$ closely match that of the orthorhombic MoO_3 (JCPDS reference card no. 05-0508). However, the treatment at 180 °C caused the phase transformation from orthorhombic MoO_3 to monoclinic MoO_2 (JCPDS reference card no. 78-1071). Fig. 1e shows the (020) peaks of all samples. The changes in *b* lattice parameter of α-MoO_3 can be calculated by the change in the position of the (020) peak, which increases from 13.80 Å for MoO_{3-x} to 14.12 Å for $MoO_{3-x}-120$ and $MoO_{3-x}-150$. This means that the reduction results in the increasing interlayer spacing of the oxide, which can facilitate Li intercalation and transport. Transmission electron microscopy (TEM) imaging was performed along the [010] crystal orientation (Fig. S3). According to the selected area electron diffraction (SAED) of MoO_{3-x} and $MoO_{3-x}-120$, the crystal face (010) kept its structure after the reduction. It is inferred that the ethanol more easily reacts with oxygen shared by neighboring octahedra of two bilayers. With the temperature rising, the kinetic control of ethanol reduction changes to the thermodynamics one and ethanol begins to react with the oxygen between the Mo atoms of the same (010) layer. Therefore, it was concluded that a reduction temperature of 120 °C is the optimum choice, since $MoO_{3-x}-120$ crystals keep the layered structure of MoO_{3-x} with enhanced interlayer spacing, but no cracking of MoO_2 formation occurs.

To confirm the enhanced ionic conductivity of the samples after reduction, electrochemical performance of the MoO_{3-x}, $MoO_{3-x}-120$ and $MoO_{3-x}-150$ was studied systematically in a three-electrode configuration in a potential window of −1.6 V to 0.4 V vs. Ag/AgCl (1.5 V to 3.5 V vs, Li/Li^+) in an electrolyte of 1 M $LiClO_4$ in 1:1 mixture of ethylene carbonate and dimethyl carbonate. All electrodes were fabricated by vacuum filtration of a mixture of MoO_{3-x} and carbon nanotube (CNT) at 4:1 ratio, resulting in freestanding and binder-free electrodes. The electrodes with 20 wt% CNT content show an electrical conductivity of 4 S/cm which is much higher than the conductivity of the electrodes without CNTs ($< 10^{-5}$ S/cm), measured by the four-point probe method. Fig. 2a shows the CV curves of different electrodes recorded at 20 mV/s. As explained by Augustyn et al. [34], a charging time ranging from 10 s to 10 min is appropriate for intercalation pseudocapacitor materials and devices performing on this timescale can bridge the gap between batteries and EDLCs. We recorded CV curves at 20 mV/s, which is equivalent to 100 s charging time for the 2 V voltage window. The CV curve of CNT-$MoO_{3-x}-120$ clearly shows Li intercalation (A) and deintercalation (B) peaks. These peaks are broader and smaller in the case of CNT-$MoO_{3-x}-150$ and almost entirely disappear in the case of untreated CNT-MoO_{3-x}. The potential difference between the intercalation and deintercalation peaks is 0.34 V for $MoO_{3-x}-120$ and increases to 0.68 V in the case of $MoO_{3-x}-150$, which is a

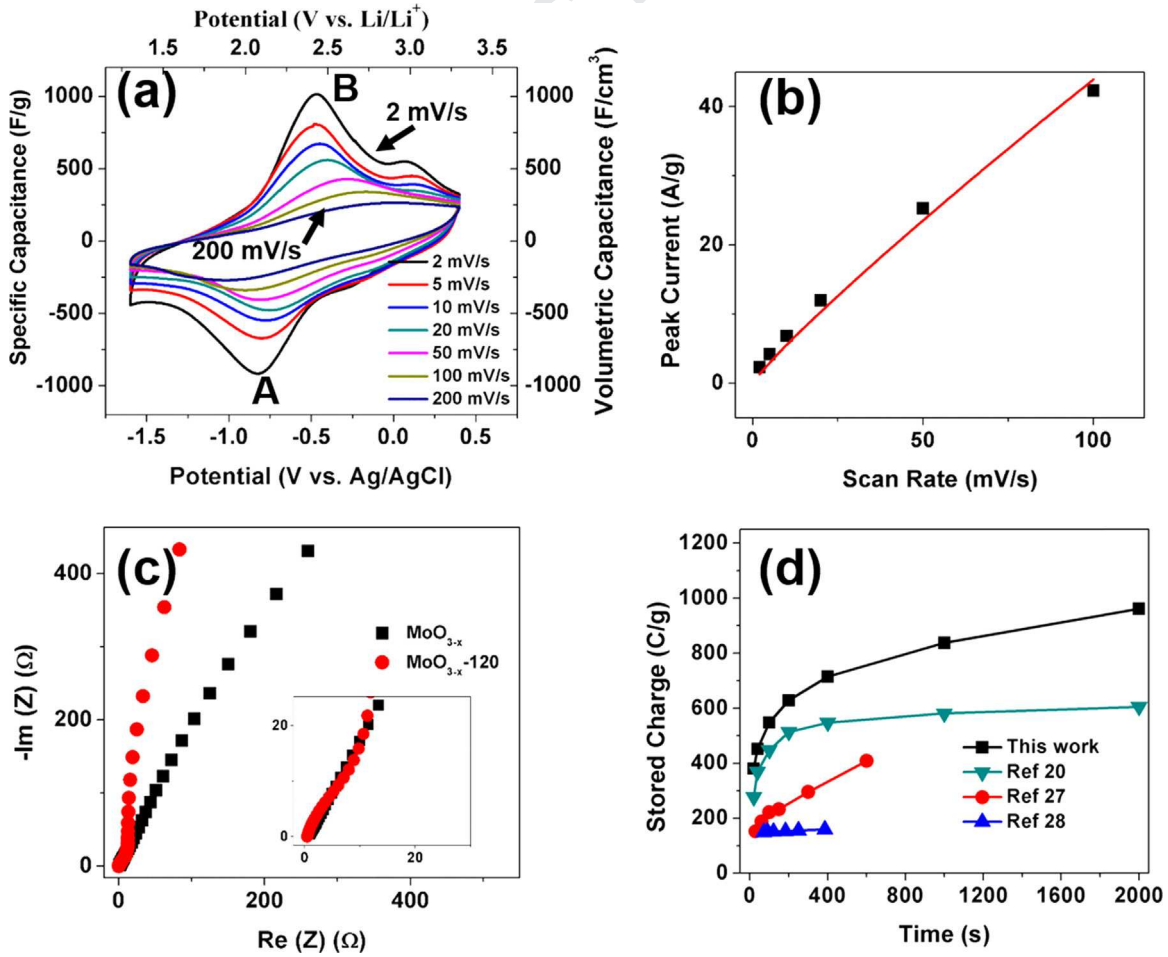

Fig. 3. (a) Cyclic voltammograms of CNT-$MoO_{3-x}-120$ from 2 mV/s to 200 mV/s. (b) The peak current of peak A vs. the scan rate. (c) The Nyquist plots for $MoO_{3-x}-120$. (d) The charge storage capability of CNT-$MoO_{3-x}-120$ compared with previously reported materials.

Please cite this article as: T. Li, et al., Ethanol reduced molybdenum trioxide for Li-ion capacitors, Nano Energy (2016), http://dx.doi.org/10.1016/j.nanoen.2016.05.004

sign of a better reversibility in the former case. As Fig. S1c shows, the nanobelts were cracked at 150 °C, leading to poor contact between MoO_{3-x}−150 nanobelts and CNTs, which is probably the reason for smaller and broader peaks for MoO_{3-x}−150 compared to MoO_{3-x}−120. At lower scan rates, the intercalation peaks in CVs became sharper with a smaller difference between intercalation and deintercalation potentials (Fig. S7a). Fig. 2b shows the calculated specific capacitances of all samples at various scan rates. At a low scan rate of 2 mV/s, the specific capacitance values of CNT-MoO_{3-x}−120 and CNT-MoO_{3-x}−150 are 418 F/g and 375 F/g, respectively, which are much higher than the specific capacitance of the untreated sample (182 F/g). The similar (010) peaks in XRD patterns of CNT-MoO_{3-x}−120 and CNT-MoO_{3-x}−150 (Fig. 1d), can be interpreted as similar interlayer spacings for these samples. Therefore, under a slow scan rate of 2 mV/s there is only a small difference in their specific capacitances. However, as the scan rate increases to 200 mV/s, specific capacitance of CNT-MoO_{3-x}−120 (152 F/g) becomes about two times higher than CNT-MoO_{3-x}−150 (79 F/g). This is related to a lower electronic conductivity of cracked CNT-MoO_{3-x}−150 (shorter belt length). The untreated CNT-MoO_{3-x} shows a much lower capacitance (182 F/g at 2 mV/s), which constantly decreases to a very small value of 19 F/g at 200 mV/s. This indicates that the untreated CNT-MoO_{3-x} samples should be mainly regarded as a Li-ion battery electrode material and cannot be used at rates expected from Li-ion capacitors.

We further studied the kinetics of Li intercalation into CNT-MoO_{3-x}−120 samples following a method suggested by Dunn et al. to distinguish surface- and diffusion-controlled responses of pseudocapacitive materials [20,35,36]. CV curves of CNT-MoO_{3-x}−120 samples at scan rates ranging from 2 mV/s to 200 mV/s are shown in Fig. 3a. The following equation was used to analyze the CV discharge peak position:

$$i = av^n \quad (1)$$

where i is current at peak position, v is scan rate, a and n are adjustable values. n value of 0.5 corresponds to a diffusion-controlled process and $n=1$ means that the process is surface-controlled. Theoretically the n value for an ideal capacitor should be equal to one, but in practice it is less than one due to the effects of ion diffusion and/or ohmic contribution. As Fig. 3b shows, for CNT-MoO_{3-x}−120 the n value was about 0.9 (nonlinear curve

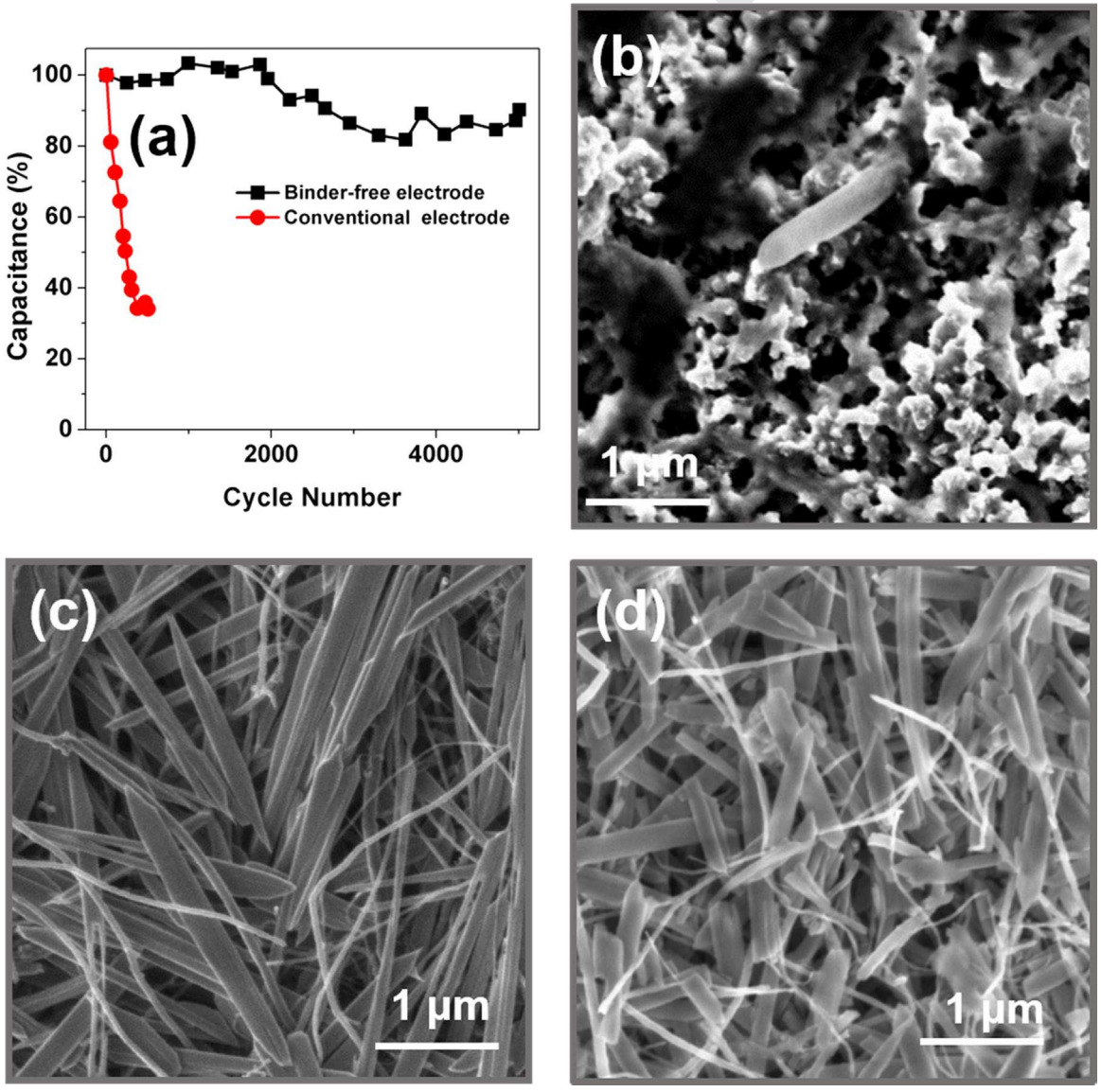

Fig. 4. (a) The cycle life testing of MoO_{3-x}−120 in the traditional (mixed with 5 %wt PVDF and 25 %wt carbon black) electrode and binder-free electrode. (b) SEM images of the electrode with binder after 500 cycles. (c) and (d) SEM images of binder-free electrode before and after 5000 cycles.

Please cite this article as: T. Li, et al., Ethanol reduced molybdenum trioxide for Li-ion capacitors, Nano Energy (2016), http://dx.doi.org/10.1016/j.nanoen.2016.05.004

fitted from 2 to 100 mV/s), which means a surface-controlled process is dominant at all scan rates. As explained by Dunn et al. [35], the current response of the electrodes at a fixed potential can be expressed as the as combinations of the contributions of the surface-controlled capacitive processes and diffusion-controlled processes according to:

$$i(V) = k_1 v^{1/2} + k_2 v \quad (2)$$

where $i(V)$ is the current at a specific potentials, v is scan rate. ($k_1 v$) and diffusion-controlled ($k_2 v^{1/2}$). And V is the potential at which i is measured. For analytical purposes, Eq. (2) can be rearranged to:

$$i(V)/v^{1/2} = k_1 + k_2 v^{1/2} \quad (3)$$

k_1 and k_2 can be determined from the slope and intercept of the $i(V)/v^{1/2}$ *vs.* $v^{1/2}$ graph. Fig. S5 shows this graph calculated for the CV peak current at various scan rates. k_1 and k_2 were calculated from this graph to be equal to 0.097 and 0.79, respectively. This means that about 76% of the current at peak potentials are from capacitive surface-controlled processes at 100 mV/s. This explains the high rate capability of the reduced samples as the charge storage in these samples is not limited by diffusion of ions (Fig. 2b).

The high-rate ion intercalation/deintercalation into the structure of the reduced samples can also be observed by the electrochemical impedance spectroscopy (EIS) in Fig. 3c. The high-frequency (200 kHz to 50 Hz) region of the Nyquist plot shows a smaller Warburg region related to ion diffusion resistance for the reduced sample. Its low frequency region of the Nyquist plot is much closed to a vertical line compared to that of the untreated sample, showing the excellent capacitive performance. In addition, the characteristic frequency of the reduced electrodes (f_0) was calculated to be about 4 Hz from the impedance data. The relaxation time constant ($\tau_0 = 1/f_0$, where f_0 is characteristic frequency) (Fig. S4b) of the electrodes was about 250 ms, which is lower than relaxation time constant of commercial activated carbon electrodes (~1 s). The ion diffusion coefficient could also be calculate from EIS, which changed from 9.034×10^{-11} cm^2/s for the as-synthesized material to 1.992×10^{-9} cm^2/s for the reduced MoO_{3-x}−120 (Fig. S6). In order to compare the performance of electrodes with other reports in the literature [20,27,28], the calculated specific capacitance was converted to the specific charge (Q) using the equation $Q = CV$. As shown in Fig. 3(d), the CNT-MoO_{3-x}−120 electrode shows a higher stored charge compared to other MoO_{3-x} based electrodes reported in the literature for all discharging times. The MoO_{3-x}−120 reached a specific charge of 961 C/g at a scan rate of 1 mV/s (2000 s charge/discharge time), which is very close to the theoretical capacity of MoO_{3-x} (1005 C/g, assuming 1.5 Li/Mo in MoO_3). It is worth noting that for some reported data in the literature, for example Ref. [20], electrodes with very a low mass loading were used for the electrochemical experiments. However, electrodes reported here with a mass loading in excess of 0.5 mg/cm^2, still show a good electrochemical performance. At scan rates of 2 mV/s and 20 mV/s, the Coulombic efficiency was about 94% and 100%, respectively (Fig. S4c). Fig. S4d displays the galvanostatic cycling with potential limitation (GCPL) of the samples. Supporting CV measurements, GCPL tests also show the excellent capacitive performance of the electrodes. The charge and discharge profiles show shoulders corresponding to the peaks observed in the CV curves.

To understand the effect of the electrode structures and fabrication methods on their electrochemical performance, we compared electrochemical behavior of freestanding MoO_{3-x}−120/CNT electrodes to conventional electrodes fabricated by pasting a mixture of the 75% active material, 5% PVDF as binder, and 25% carbon black as conductive additive on aluminum foil. Both types of electrodes display good capacitance at low scan rates. Conventionally conventional electrodes with carbon black show a specific capacitance of about 370 F/g at 2 mV/s scan rate compared to the specific capacitance of about 418 F/g for binder-free electrodes at the same scan rate. Nonetheless, when the scan rate increased to 200 mV/s, the specific capacitance of the conventional samples dropped to 70 F/g (Fig. S7b), which is much lower than the specific capacitance of the freestanding and binder-free samples (152.6 F/g at 200 mV/s scan rate). Cycling stability of the samples was also heavily influenced by the electrode structure and preparation method. In order to demonstrate the importance of uniform electronic conductivity in the electrodes, the two types of electrodes were subjected to 5000 cycle tests by GCPL at a current density of 5 A/g. As shown in Fig. 4a, the traditionally fabricated electrode lost 70% of its initial capacitance after 500 cycles, while the binder-free electrode retained 90% of its initial capacitance after 5000 cycles. The morphologies of both electrodes were examined by SEM before and after cycling. The inhomogeneous distribution of carbon black particles (conductive additive in conventionally made electrode) and partial contact between the particles and nanobelts (Fig. S8) results in an uneven lithium intercalation and electrode expansion of MoO_3 nanobelts, leading to their cracking and mechanical failure during consecutive cycling. The binder may also affect the fracture of electrodes as uneven distribution of binder on the surface of nanobelts may result in an uneven volume expansion. In other words, parts of the nanobelts that are covered with binder are more constrained and expand less during Li intercalation. Consequently, this results in transformation of nanobelts to nanoparticles after 500 cycles (as shown in SEM image of Fig. 4b). In contrast, the binder-free electrodes, which are free to move during expansion/contraction while being charged/discharged, keep their initial morphology after 5000 charge and discharge cycles (Fig. 4c and d). The high conductivity of CNTs in the network of CNTs and MoO_3 nanobelts results in a uniform polarization and expansion of the electrodes during charging. Moreover, the increased conductivity of the electrodes promotes their rate capability, as discussed above.

The results presented here illustrate the benefits from both, improved ion diffusion and electron transport in the partially reduced MoO_{3-x} (x=0.06–0.43) electrode that are required for rapid charging of electrodes [37]. The enhanced capacitance, rate capability and cyclic performance of the electrode are the results of (1) increased Li ion intercalation/deintercalation rates due to a larger interlayer spacing (from 13.80 Å to 14.12 Å) in the oxide structure, and (2) fast electron transport in the electrodes as a result of formation of a CNT/MoO_{3-x} network. The best performance was achieved for samples reduced at 120 °C (MoO_{3-x} −120) that showed excellent capacitive behavior at a high scan rate in organic electrolyte (152 F/g at 200 mV/s). The importance of the CNT addition for uniform polarization of the electrode and its effects on cyclic stability of the electrodes has been shown.

Acknowledgement

The work performed at Drexel University was supported by the Q6 Fluid Interface Reactions, Structures and Transport (FIRST) Center, an Energy Frontier Research Center funded by the U.S. Department of Energy, Office of Science, Office of Basic Energy Sciences. The work at WNLO was financially supported by the National Natural Science Foundation of China (51322210 and 61434001) and Director Fund of WNLO. The authors also thank Dr. J. Su and Dr. Z. Ling for experimental help. The authors also acknowledge support of the Analysis and Testing Center of Huazhong University of Science and Technology.

Appendix A. Supplementary material

Supplementary data associated with this article can be found in the online version at http://dx.doi.org/10.1016/j.nanoen.2016.05.004.

References

[1] J.R. Miller, P. Simon, Science 321 (2008) 651–652.
[2] P. Simon, Y. Gogotsi, Nat. Mater. 7 (2008) 845–854.
[3] E. Frackowiak, F. Béguin, Carbon 39 (2001) 937–950.
[4] P. Simon, Y. Gogotsi, B. Dunn, Science 343 (2014) 1210–1211.
[5] B.E. Conway, Electrochemical Supercapacitors: Scientific, Fundamentals And Technological Applications, Plenum, New York, 1999.
[6] H.S. Teng, Y.J. Chang, C.T. Hsieh, Carbon 39 (2001) 1981–1987.
[7] D. Pech, M. Brunet, H. Durou, P. Huang, V. Mochalin, Y. Gogotsi, P.L. Taberna, P. Simon, Nat. Nano 5 (2010) 651–654.
[8] M. Armand, J.M. Tarascon, Nature 451 (2008) 652–657.
[9] A.K. Padhi, K.S. Nanjundaswamy, J.B. Goodenough, J. Electrochem. Soc. 144 (1997) 1188–1194.
[10] T. Sakai, H. Ishikawa, K. Oguro, C. Iwakura, H. Yoneyama, J. Electrochem. Soc. 134 (1987) 558–562.
[11] S.R. Ovshinsky, M.A. Fetcenko, J. Ross, Science 260 (1993) 176–181.
[12] Z. Yang, J. Zhang, M.C.W. Kintner-Meyer, X. Lu, D. Choi, J.P. Lemmon, J. Liu, Chem. Rev. 111 (2011) 3577–3613.
[13] J.M. Tarascon, M. Armand, Nature 414 (2001) 359–367.
[14] M. Toupin, T. Brousse, D. Bélanger, Chem. Mater. 16 (2004) 3184–3190.
[15] J. Jiang, A. Kucernak, Electrochim. Acta 47 (2002) 2381–2386.
[16] T. Brousse, M. Toupin, R. Dugas, L. Athouël, O. Crosnier, D. Bélanger, J. Electrochem. Soc. 153 (2006) A2171–A2180.
[17] M. Acerce, D. Voiry, M. Chhowalla, Nat. Nano 10 (2015) 313–318.
[18] Z. Ling, C.E. Ren, M.-Q. Zhao, J. Yang, J.M. Giammarco, J. Qiu, M.W. Barsoum, Y. Gogotsi, Proc. Natl. Acad. Sci. USA 111 (2014) 16676–16681.
[19] M.R. Lukatskaya, O. Mashtalir, C.E. Ren, Y. Dall'Agnese, P. Rozier, P.L. Taberna, M. Naguib, P. Simon, M.W. Barsoum, Y. Gogotsi, Science 341 (2013) 1502–1505.
[20] T. Brezesinski, J. Wang, S.H. Tolbert, B. Dunn, Nat. Mater. 9 (2010) 146–151.
[21] L.Q. Mai, B. Hu, W. Chen, Y.Y. Qi, C.S. Lao, R.S. Yang, Y. Dai, Z.L. Wang, Adv. Mater. 19 (2007) 3712–3716.
[22] J.S. Chen, Y.L. Cheah, S. Madhavi, X.W. Lou, J. Phys. Chem. C 114 (2010) 8675–8678.
[23] Z. Wang, S. Madhavi, X.W. Lou, J. Phys. Chem. C 116 (2012) 12508–12513.
[24] X. Xiao, T. Ding, L. Yuan, Y. Shen, Q. Zhong, X. Zhang, Y. Cao, B. Hu, T. Zhai, L. Gong, J. Chen, Y. Tong, J. Zhou, Z.L. Wang, Adv. Energy Mater. 2 (2012) 1328–1332.
[25] X. Xiao, Z. Peng, C. Chen, C. Zhang, M. Beidaghi, Z. Yang, N. Wu, Y. Huang, L. Miao, Y. Gogotsi, J. Zhou, Nano Energy 9 (2014) 355–363.
[26] X. Xiao, C. Zhang, S. Lin, L. Huang, Z. Hu, Y. Cheng, T. Li, W. Qiao, D. Long, Y. Huang, L. Mai, Y. Gogotsi, J. Zhou, Energy Storage Mater. 1 (2015) 1–8.
[27] Q. Mahmood, H.J. Yun, W.S. Kim, H.S. Park, J. Power Source 235 (2013) 187–192.
[28] L.S. Aravinda, U. Bhat, B. Ramachandra Bhat, Electrochem. Acta 112 (2013) 663–669.
[29] I. Shakir, M. Shahid, H.W. Yang, D.J. Kang, Electrochem. Acta 56 (2010) 376–380.
[30] J. Jiang, J. Liu, S. Peng, D. Qian, D. Luo, Q. Wang, Z. Tian, Y. Liu, J. Mater. Chem. A 1 (2013) 2588–2594.
[31] X. Xiao, X. Peng, H. Jin, T. Li, C. Zhang, B. Gao, B. Hu, K. Huo, J. Zhou, Adv. Mater. 25 (2013) 5091–5097.
[32] R. Tokarz-Sobieraj, K. Hermann, M. Witko, A. Blume, G. Mestl, R. Schlögl, Surf. Sci. 489 (2001) 107–125.
[33] X.K. Hu, Y.T. Qian, Z.T. Song, J.R. Huang, R. Cao, J.Q. Xiao, Chem. Mater. 20 (2008) 1527–1533.
[34] V. Augustyn, P. Simon, B. Dunn, Energy Environ. Sci. 7 (2014) 1597–1614.
[35] J. Wang, J. Polleux, J. Lim, B. Dunn, J. Phys. Chem. C 111 (2007) 14925–14931.
[36] L.M. Doubova, A. De Battisti, S. Daolio, C. Pagura, S. Barison, R. Gerbasi, G. Battiston, P. Guerriero, S. Trasatti, Russ. J. Electrochem, 40, pp. 1115–1122.
[37] S. Lee, J. Cho, Angew. Chem. Int. Ed. 54 (2015) 2–6.

Please cite this article as: T. Li, et al., Ethanol reduced molybdenum trioxide for Li-ion capacitors, Nano Energy (2016), http://dx.doi.org/10.1016/j.nanoen.2016.05.004